



# HF radar-derived origin and destination of surface waters off Bodega Bay, California

David M. Kaplan<sup>a,\*</sup>, John Largier<sup>b</sup>

<sup>a</sup>*Wildlife, Fish and Conservation Biology, University of California, 1 Shields Ave., Davis, CA 95616, USA*

<sup>b</sup>*Bodega Marine Lab, University of California, Davis, P.O. Box 247, Bodega, CA 94923, USA*

Received 5 March 2005; accepted 9 July 2006

Available online 20 November 2006

## Abstract

As an integral part of the WEST study of the role of wind-driven transport in shelf productivity, HF radar currents are analyzed to determine typical surface flow patterns off Bodega Bay in northern California. Radar-derived surface trajectories and surface velocity divergences are used to determine the proximal origins and destinations of surface waters in the area. Surface trajectory results show a strong bimodality, with water over the entire shelf originating in the north under upwelling conditions and waters over the inner/mid-shelf originating in the south during relaxation conditions. Outer shelf waters have more variable transport patterns during relaxation conditions, with limited equatorward or onshore movements being most typical. The destinations of surface waters starting at the outer shelf are predominantly offshore, with the majority of particles exiting the radar domain west of Pt Reyes along the shelf edge in less than 2 days. Significant proportions of water from the inner/mid-shelf are exported southward and exit the radar domain inshore or within 20 km of the tip of Pt Reyes, creating possibilities for either nearshore retention in the Bodega region or entrainment of water into the Gulf of Farallons. Approximately 15% of all trajectories remained in the radar domain for 6 days, suggesting that a biologically significant percentage of larvae might be retained in the area for time periods approaching typical larval durations. Calculations of surface divergence indicate where vertical flux may be significant. An extensive area of positive divergence is observed off Bodega during upwelling conditions, while weakly convergent flow is observed where upwelling flows approach Pt Reyes. Positive divergence also is observed during relaxation periods when poleward flow separates from the shore just north of Pt Reyes. Estimates of vertical flux in these divergence zones point to a significant contribution of recently upwelled waters to the observed horizontal fluxes at the surface. Determination of the ultimate source and fate of phytoplankton-rich waters requires further analysis of the detailed time dependence of phytoplankton concentration relative to the time dependence of wind-forced currents.

© 2006 Elsevier Ltd. All rights reserved.

**Keywords:** Transport processes; Upwelling and relaxation; Wind-driven currents; Oceanic divergences; Surface currents; Radio oceanography

## 1. Introduction

The objective of the WEST program is to obtain a better understanding of the role of wind-driven transport in shelf productivity. Specifically, while we

\*Corresponding author.

*E-mail address:* [dmkaplan@ucdavis.edu](mailto:dmkaplan@ucdavis.edu) (D.M. Kaplan).

<sup>1</sup>Current address: Institute of Marine Sciences, UCSC/Ocean Sciences, 1156 High Street, Santa Cruz, CA 95064, USA.

know that upwelling of high-nutrient subsurface waters results in phytoplankton blooms, and that these blooms occur during periods of relaxation following upwelling (e.g., Fig. 1), it is not possible to assess the source nor the fate of these blooms without knowing more about the movement of surface waters in an upwelling area like that off Bodega Bay. The deployment of HF surface radars in the area in 2001 provided the data on surface currents necessary for an analysis of the source and fate of surface waters sampled at the key WEST sites off Bodega Bay.

This paper follows a paper by Kaplan et al. (2005) in which the HF radar data were analyzed as Eulerian data and the focus was on the structure and dynamics of surface flows over the shelf. In that paper, we describe a strong cross-shore gradient in the strength of alongshore currents, as well as strong gradients in tidal and inertial flow energy. Wind-driven currents over the outer shelf and slope tend to be strong and persistently equatorward, whereas nearshore currents are as often poleward as equatorward. Point Reyes is an important barrier to alongshore flow, producing an offshore deflection

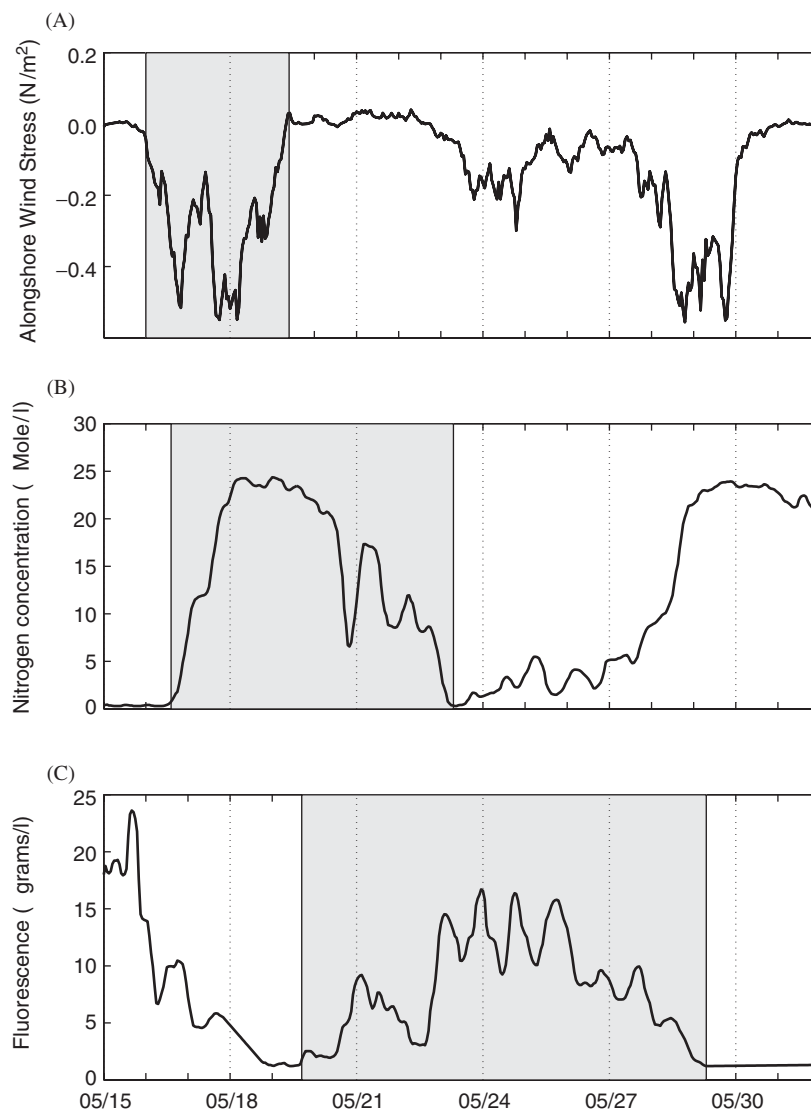


Fig. 1. Alongshore wind stress (A), dissolved nitrogen concentration (B) and fluorescence (C) for the second half of May 2001. Wind measurements were made at NDBC 46013. Nitrogen concentration and fluorescence were measured at the D90 WEST mooring at 1 m depth. Gray areas indicate a wind event (A), followed shortly by high nutrient levels (B), which in turn were followed by a phytoplankton bloom (C).

of the equatorward upwelling jet. During periods of relaxation of upwelling winds, there is a strong poleward current that moves around Pt Reyes within 20 km of the peninsula. Several papers in this volume contribute to this improving picture of the detailed structure of wind stress (Dorman et al., 2006), surface divergence (Dever et al., 2006), and phytoplankton blooms (Wilkerson et al., 2006). In this work, the spatial continuity of the radar data is used to calculate quasi-Lagrangian trajectories and the focus is on transport patterns—where does water come from and where does it go to?

## 2. Data and methods

This paper is focused on the quasi-Lagrangian data that can be derived from the array of 95 Eulerian data obtained from radar measurements of surface currents (see below). In our previous work (Kaplan et al., 2005), we used the Eulerian data directly. Here we focus on the potential for surface maps of current to yield surface trajectories that are not available from moorings that are too sparse in space, or from drifters that are too sparse in time. However, it should be remembered that the surface map does not capture 3-dimensional flow, and thus it will indicate trajectories that deviate from the real trajectory where there is a vertical flux and it will not capture the effect of shear dispersion. To explore where vertical fluxes may be considerable, we use the surface data to identify regions where divergence/convergence is strong. Furthermore, we focus our attention on the mean pathways and resist the temptation to describe individual trajectories or to address the diffusive effects associated with small-scale motion. With these qualifications, we proceed cautiously to use surface flow patterns as representative of trajectories of water parcels in this paper.

### 2.1. HF radar data

The HF radar data used in this study are from an array of three CODAR Ocean Sensors SeaSonde antennas located along the coast of north-central California at Pt Reyes, Bodega Marine Laboratory (BML; on Bodega Head) and Gerstle Cove (Fig. 2). Each antenna operated at a central frequency of 12.5 MHz, giving them a horizontal range for radial current measurements of 50–70 km. Vector surface current velocities were calculated on a 2 km × 2 km grid over an area that extended approximately

55 km in the offshore direction and 80 km in the along-shore direction. We required a minimum of three radial vectors from at least two different radar sites for the calculation of a vector current velocity at a grid point. Vector currents were rejected if they were greater than 1.0 m s<sup>-1</sup> or they had a geometric dilution of precision (GDOP: Wells and Beck, 1987; Chapman and Graber, 1997) greater than 2. We also used a second estimation of the error in a vector current that is similar to the mapping error but takes into account the measured variability in the radial currents (Lipa, 2003). If this error vector was greater than 0.18 m s<sup>-1</sup> in magnitude then the current estimate for that grid point was omitted. Finally, grid points were only included if valid total current vectors are available more than 40% of the time.

HF radar data are available, with some data gaps, from May 2001 till the present. The principal focus of this study is the spring/summer upwelling season of 2003, during which time all three radars were operational and radar coverage was at its maximum extent.

### 2.2. Virtual particle tracks

Virtual particle tracks derived from HF radar currents were calculated using a second-order method with a variable time step (Bennett and Clites, 1987). The size of the time step was adjusted so that no particle moved more than 0.25 km (one-eighth of the grid spacing) in a single time step. The maximum time step was 1 h. The second-order method produced particle tracks very similar to a first-order algorithm with a fixed 1-h time step, suggesting that little improvement would be obtained by using a higher-order algorithm.

We have not included any additional diffusive terms in the particle-tracking algorithm to account for small-scale spatial and temporal current variability. Our HF radar data have a spatial resolution of 2 km and a temporal resolution of 1 h. These spatial and temporal scales are sufficient to capture tidal, inertial, diurnal and subtidal variability in currents (Kaplan et al., 2005), although they would miss some small-scale variability. The HF radar data themselves have an intrinsic noise that is on the order of 0.05–0.15 m s<sup>-1</sup> (Kaplan et al., 2005), which introduces a diffusive effect. We have compared the actual tracks of drifters (6-m drogues extending from 4.5 to 10.5 m depth) released in or near the radar domain in 2001 to particle tracks generated

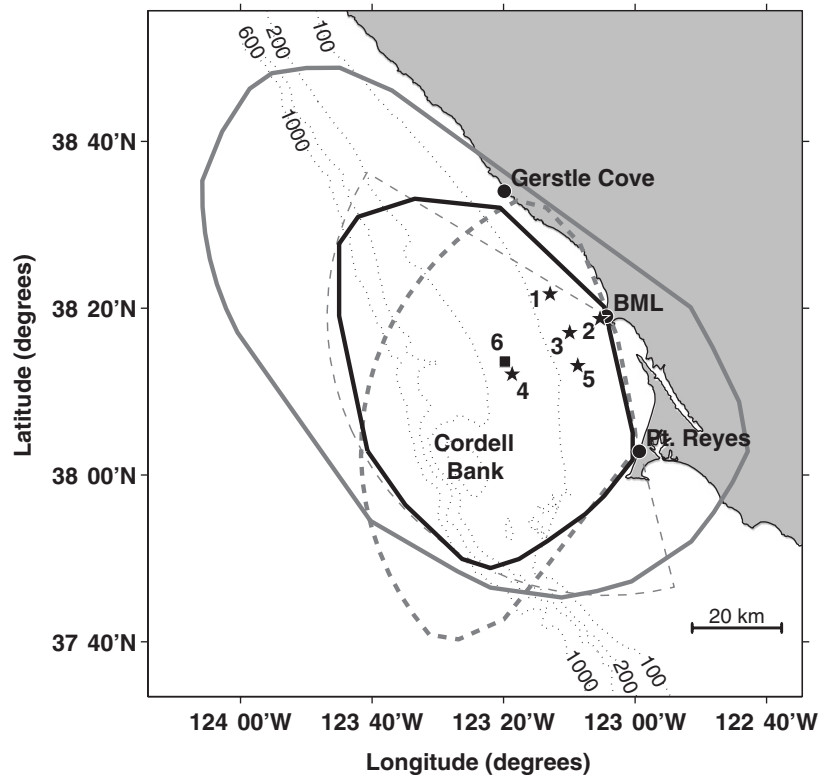


Fig. 2. Coverage areas of radial and total currents from three radar stations used in this study. The three black dots along the coast indicate the locations of the radar antenna. Gray lines indicate coverages of radial currents from Bodega Marine Laboratory (BML; thin-dashed line), Point Reyes (thick-dashed line) and Gerstle Cove (thick-solid line) radars. The dark line shows the resulting coverage of total vector currents in the area of signal overlap. The positions of the WEST and NDBC moorings are numbered as follows: (1) E90, (2) D40, (3) D90, (4) D130, (5) C90 and (6) NDBC 46013 buoy. Note that the D90 and D130 moorings are located close to the D2 and D3 sampling stations, respectively, where repeated biological measurements were made during cruises from 2000 to 2002.

from HF radar data at the same time (Kaplan et al., 2005). Quasi-Eulerian drifter speeds had an RMS difference with respect to HF radar currents on the order of  $0.13 \text{ m s}^{-1}$ , and separation rates between real and pseudo-drifters were between 1 and  $10 \text{ km day}^{-1}$  with a mean value around  $5 \text{ km day}^{-1}$  (Fig. 3). HF radar currents ( $<1 \text{ m}$ ) had a tendency towards larger speeds than those observed in the drifter data ( $>5 \text{ m}$ ), consistent with surface wind forcing and horizontal shear with depth. Though the differences between radar and drifter trajectories are considerable, there was no strong directionality to them. To minimize the impact of these differences on the results in this paper, the primary focus here will be on average spatial 160 and temporal transport patterns.

Particles were released from four different locations inside the radar domain (Fig. 4). Two of the areas were 5-km-radius circles near Bodega Head on the 90 and 130 m isobaths at the locations of the

D90 and D130 WEST moorings. These zones contained 18 and 19 HF radar grid points, respectively, and will be referred to as the “inner shelf zone” and the “outer shelf zone”. The other zones were along the southern edge of the radar domain (also 5-km-radius circles)—these are referred to as the “Reyes inshore” and “Reyes offshore” zones. Particles were released eight times a day beginning at midnight GMT-8 (i.e. PST with no daylight savings) from all HF radar grid points inside each patch. Each particle was followed for a period of up to 6 days.

When particles moved out of the HF radar data region, their final location and time of exit were recorded. The exit point of each particle was associated with the nearest point on the border curve shown in Fig. 4. This border curve was divided into 100 equidistant sections, and the total number of particles exiting in each section and the average time-to-exit were calculated.

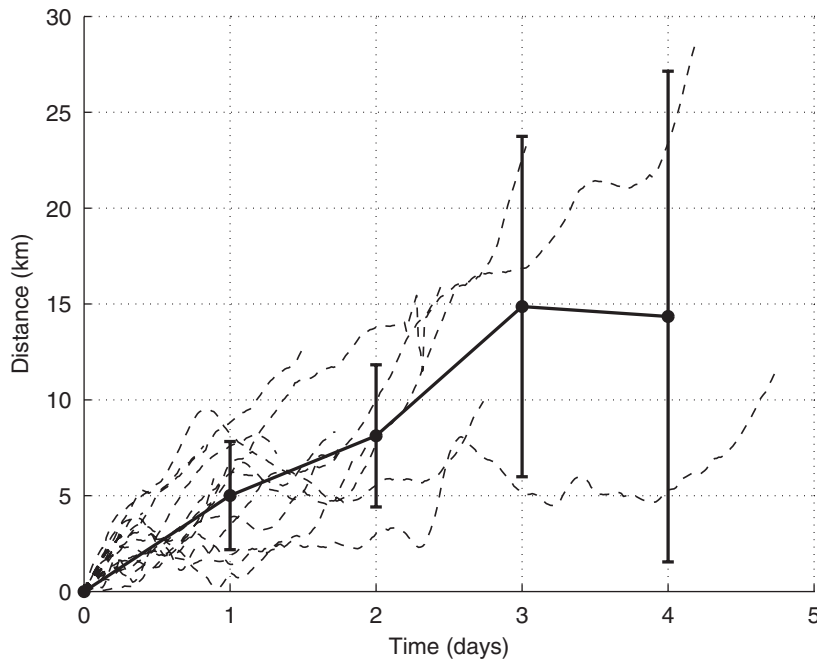


Fig. 3. Separation between drifter and HF-radar tracks as a function of time. Gray, dashed lines show the separations of individual pairs of drifter and HF-radar tracks. The solid line gives the mean at 24-h intervals and the standard deviation around the mean.

Here and elsewhere in this work, we group results into upwelling and relaxation categories, according to the strength of the subtidal alongshore wind stress (i.e. wind stress measured at the NDBC 46013 buoy and then filtered with the PL64 filter; see Section 2.5). Periods with principal axis wind stress that is equatorward and greater in magnitude than  $0.15 \text{ N m}^{-2}$  ( $10.3 \text{ m s}^{-1}$  at 10 m height) are labeled as upwelling. Time periods with a wind stress magnitude less than  $0.05 \text{ N m}^{-2}$  ( $6.0 \text{ m s}^{-1}$  at 10 m height) are considered to be relaxation periods. All other times were considered transition periods.

### 2.3. Reverse particle tracks

We also calculated reverse particle tracks, i.e. tracks of where a parcel of water was at some time in the past. Reverse particle tracks were found by first calculating forward particle tracks from a large number of grid points and then keeping those tracks that fell within a certain distance of the location(s) of interest at the specified time. This process can be seen in Fig. 5, which shows particle tracks emanating from all grid points for a 6 h time period in June 2003. Tracks shown in red are within 5 km of the point of interest and the grid points shown in

green show the location of these surface waters 6 h earlier.

From a selected set of HF radar points along the border of the radar domain (Fig. 6), water parcels were released eight times a day and followed for a period of up to 4 days. Every hour we checked for particles that had reached one of the target patches. Two target regions were considered, corresponding to the inner shelf and outer shelf zones discussed previously.

### 2.4. Surface divergence calculations

The divergence of surface current velocities is a measure of vertical flux to/from the thin surface layer in which currents are observed by HF radar ( $< 1 \text{ m}$ ) and indicates a link between near-surface and deeper flow (i.e. upwelling, downwelling or vertical mixing). As divergence is based on the difference between currents at nearby points, it is particularly sensitive to noise and small-scale spatial variability. As such, our calculations of the surface divergence are based on subtidal, noise-filtered current vectors. Subtidal records of HF radar currents were obtained at each grid point by applying the 38-h PL64 low-pass filter (Beardsley et al., 1985) to remove tidal, diurnal and inertial

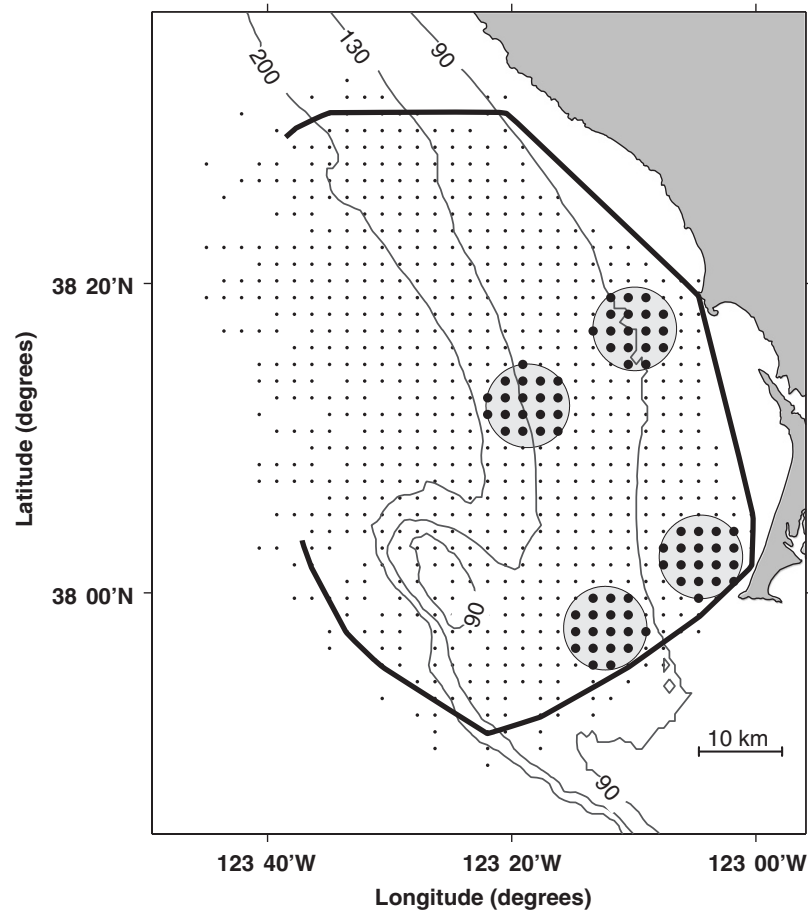


Fig. 4. Zones where particles were released. The four zones are indicated by gray circles with large, black dots at each grid point where particles were released. The upper two zones, moving left to right, are the “outer shelf” and “inner shelf” zones, respectively, while the lower two are the “Reyes offshore” and “Reyes inshore” zones. The thick, black line along the edge of the data region is the border used to define the exit points of water parcels from the data region.

fluctuations. Further, small-scale spatial variability and noise in the subtidal currents were removed by calculating empirical orthogonal functions (EOF's) and then reducing the original data to the mean plus all EOF's that represented more than 2% of the total variance in the data (in this case, the top four EOF's representing 82.5% of the total variance). Before EOF calculation, current vectors at each grid point were normalized by the standard deviation of the component of the current along the principal axis of variability at that grid point. This normalization was chosen so that grid points with smaller currents and current variability, such as along the coast near Bodega Bay (Kaplan et al., 2005), had the same weighting as grid points with greater variability in the determination of the modes. This methodology is appropriate in this context as we wanted to give equal weighting to variability in all

areas of the data region. Final surface divergence maps showed little sensitivity to whether or not this normalization was applied. The normalization applied before EOF calculation was reversed after EOF calculation so that the final currents used to calculate the divergence had the same scale as the original current vectors.

The surface divergence was then calculated at each time step and grid point from these subtidal, noise-filtered current vectors. The resulting surface divergence was then grouped into upwelling and relaxation categories, according to the strength of the subtidal alongshore wind stress at each time step, as discussed in Section 2.2. The mean surface divergence was calculated at each grid point and for each category of alongshore wind stress.

The radar coverage domain does not include the open embayments from Point Reyes to Bodega

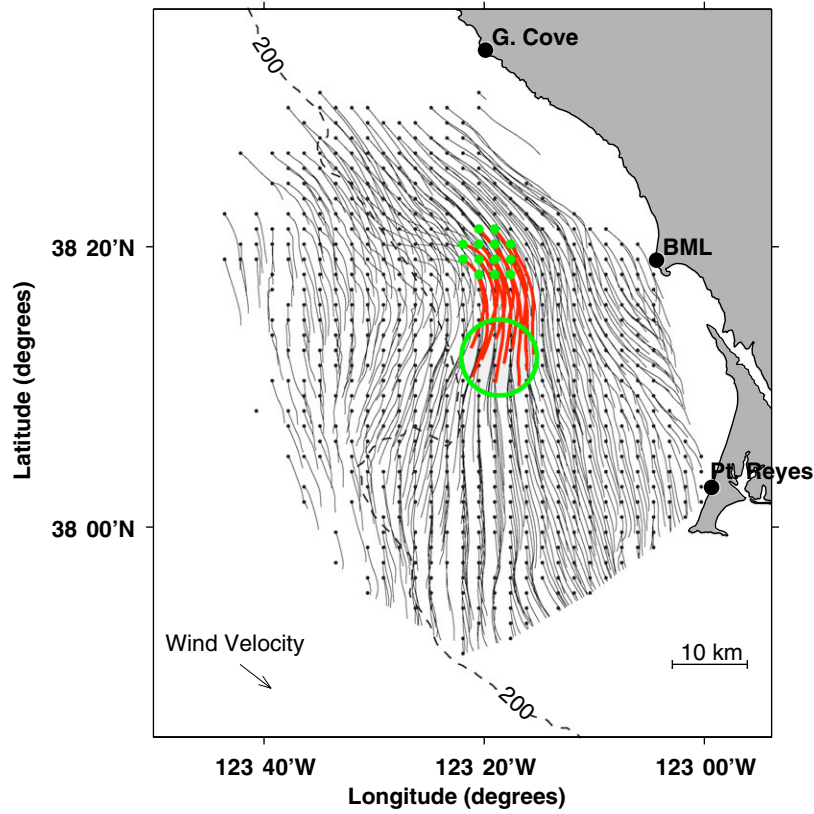


Fig. 5. Process by which “reverse” particle tracks are determined. Black lines are 6-h particle tracks for a period in June of 2003 originating from all of the radar grid points. The target region is indicated by the green circle and all tracks that landed in the circle are shown in red. The large green points are the starting points of those tracks that landed in the target region. They are considered the origins of that parcel of surface water 6 h earlier.

Head, here referred to as the Bodega embayment, and from Bodega Head to Gerstle Cove, referred to as the Russian River embayment (Fig. 6). As a proxy for direct measurement of the surface divergence in these embayments, we calculated the line integral of the subtidal current normal to the boundaries of these regions. Along each segment of the boundary curve, the average of the current at the grid points on each end was calculated. Where the boundary reached land we assumed that the current of the single seaward grid point was valid for the entire segment. The component of the current normal to the segment was calculated and the integral was computed as the sum of these normal components multiplied by the length of the segment. This integral also was divided into inward and outward fluxes (i.e. currents that were directed outwards were set to zero before performing the integral and vice-versa). These quantities were then divided by the area of the embayment to get an estimate of surface velocity divergence in the

embayment (s<sup>-1</sup>). The inward, outward and net flux per unit area of the embayment were correlated with wind stress and compared with the surface divergence from nearby grid points. Note that along the northern edge of the Russian River embayment current data are sparse, possibly causing considerable error in our estimates of surface divergence for that area.

### 2.5. Wind data

Hourly wind data are available from National Data Buoy Center (NDBC) buoy 46013, deployed at 38.23°N, 123.33°W, 25 km west of Bodega Bay (Fig. 2; <http://ndbc.noaa.gov/>). The wind stress vector, given by  $\tau = \rho C_D |w| w$ , where  $w$  is the wind speed and  $C_D$  is the coefficient of drag, was calculated from the hourly wind data with the Air–Sea Matlab toolbox (<http://sea-mat.who.edu/>). Wind velocity was corrected from 5 m recorded height to 10 m standard height and the coefficient of

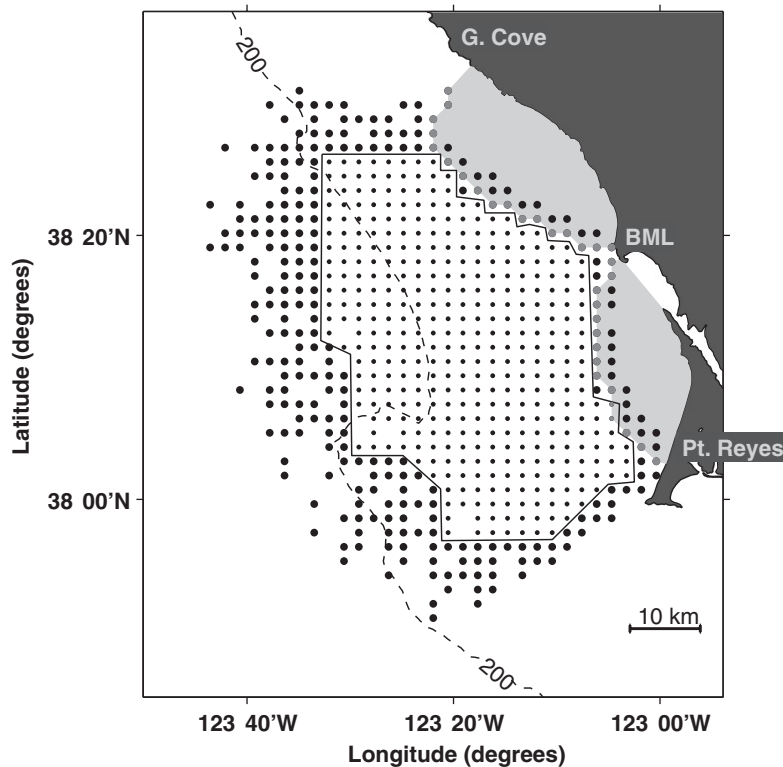


Fig. 6. Border region for determining the origin of surface water parcels. Those pseudo-particle tracks that landed inside one of the zones shown in Fig. 4 and originated at one of the grid points indicated by large dots (i.e. to the outside of the thin black line) were considered to define the trajectory of a particle from the edge of the radar domain to that zone. Also shown on the figure are two light gray areas indicating the locations of the two open embayments considered in this paper: Bodega (to the south between Pt. Reyes and BML) and Russian River (north of BML). The dark gray grid points along the border of each embayment were used to calculate the horizontal current flux in to or out of the regions.

drag used was from Large and Pond (1981). High-frequency fluctuations, including diurnal and semi-diurnal variability, were removed from the wind-stress data by applying the 38-h PL64 low-pass filter (Beardsley et al., 1985) to isolate the signal of synoptic-scale wind forcing.

### 3. Water parcel trajectories

#### 3.1. Examples of upwelling and relaxation transport patterns

HF radar-derived surface currents of the Bodega area show strong southward currents during upwelling winds and weaker northward currents over the mid/inner shelf during relaxation (Fig. 7). These spatially extensive data advance prior mooring-based descriptions (e.g., Winant et al., 1987; Largier et al., 1993) by describing in detail the spatial structure of currents in the area, including horizon-

tal shear (Kaplan et al., 2005) and the spatially heterogeneous response to different levels of wind forcing (e.g., Fig. 7). The continuity of the flow is explored here through calculation of surface transport pathways, i.e. the route that a parcel of water would follow if constrained to the surface. In general, these trajectories are linear with weak small-scale structures (Fig. 8) that are ascribed to time-dependent tidal currents (Kaplan et al., 2005).

There are significant differences among trajectories from periods with different levels of wind forcing and from different areas of the data region. During periods of strong equatorward wind forcing, current velocities over the outer shelf are on the order of  $0.2\text{--}0.5\text{ m s}^{-1}$  (of order 20–40 km in a day; Fig. 7A). Water parcels from the outer shelf zone move rapidly southward when winds are strong—for example, 20 km in 12 h on 16 July 2003 (Figs. 7A and 8B). Outer-shelf currents often remain weakly southward even when winds are weakening or

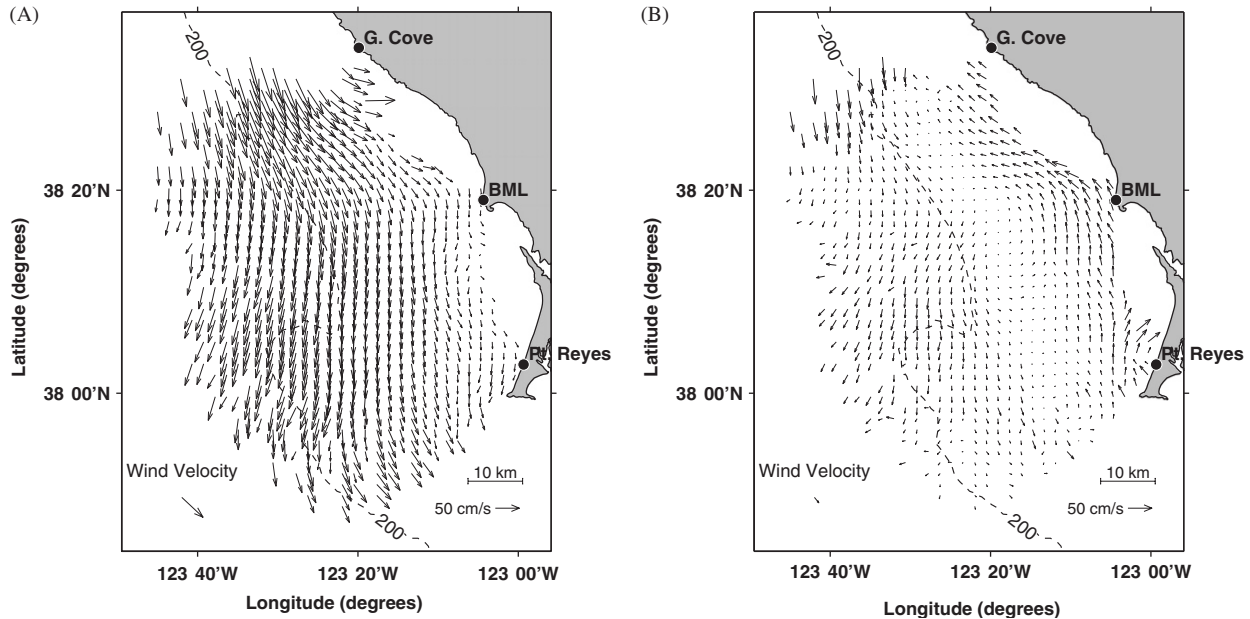


Fig. 7. Daily average surface currents from (A) 16 July 2003 and (B) 24 July 2003. On 16 July, winds were strongly upwelling favorable (NW winds of  $12.3 \text{ m s}^{-1}$  at 10 m height, i.e. wind stress of  $0.24 \text{ N m}^{-2}$ ), while on 24 July, winds were weakly upwelling favorable (NW winds of  $1.5 \text{ m s}^{-1}$ , i.e. wind stress of  $0.003 \text{ N m}^{-2}$ ).

absent (Figs. 7B and 9A), resulting in weak equatorward transport despite significantly different conditions nearshore (Figs. 8C and D). When currents are weak, tidal band variability is readily visible in the form of ellipsoidal particle trajectories (Fig. 8D). Tidal excursions are typically small relative to upwelling-driven flows (order 5–10 km), and tidal fluctuations are only noticeable as minor oscillations of otherwise linear trajectories during upwelling conditions (e.g., Fig. 8A).

This outer shelf flow pattern is in contrast to transport patterns inshore. There is a marked cross-shore gradient in alongshore transport, as water parcels over the inner shelf are advected shorter distances (order 10–20 km in a day) during upwelling conditions (Figs. 7A, 8A and B) and significant poleward flow is observed during relaxation conditions (Figs. 7B, 8D and 9B). Poleward flow is at times observed over the entire shelf during complete relaxation or reversal of the alongshore wind stress, but currents are notably stronger nearshore (Fig. 9). This cross-shore gradient in alongshore flow is more fully described in Kaplan et al. (2005). Typical velocities over the inner shelf during relaxation are of order  $0.1\text{--}0.2 \text{ m s}^{-1}$  (Fig. 9B). Convergence of trajectories is at times observed in the vicinity of

Bodega Head during relaxation (Fig. 8D), though this area is close to the line of sight between the BML and Gerstle Cove radars and currents are perhaps subject to increased error.

Also shown for relaxation conditions is transport of water from the southern boundary of the HF radar domain, near Pt Reyes (Fig. 10). A strong poleward current is observed, with strongest flows inshore (within about 10 km of the point). Speeds of up to  $0.30 \text{ m s}^{-1}$  are observed (i.e. displacements of up to 25 km in a day). Further offshore of the point, this poleward flow is weaker (order  $0.05 \text{ m s}^{-1}$ ) and comparable with tidal velocities.

### 3.2. Average transport patterns during upwelling and relaxation

The water parcel trajectories in Figs. 8 and 10 are for a single release time. A more general idea of 12-h displacements is obtained by calculating trajectories repeatedly, releasing particles every 3 h over the period from 2 May to 30 August 2003.

These trajectories are then combined to generate a probabilistic view of the destinations of water observed at the WEST D90 and D130 moorings and biological survey stations (stations D2 and D3 are

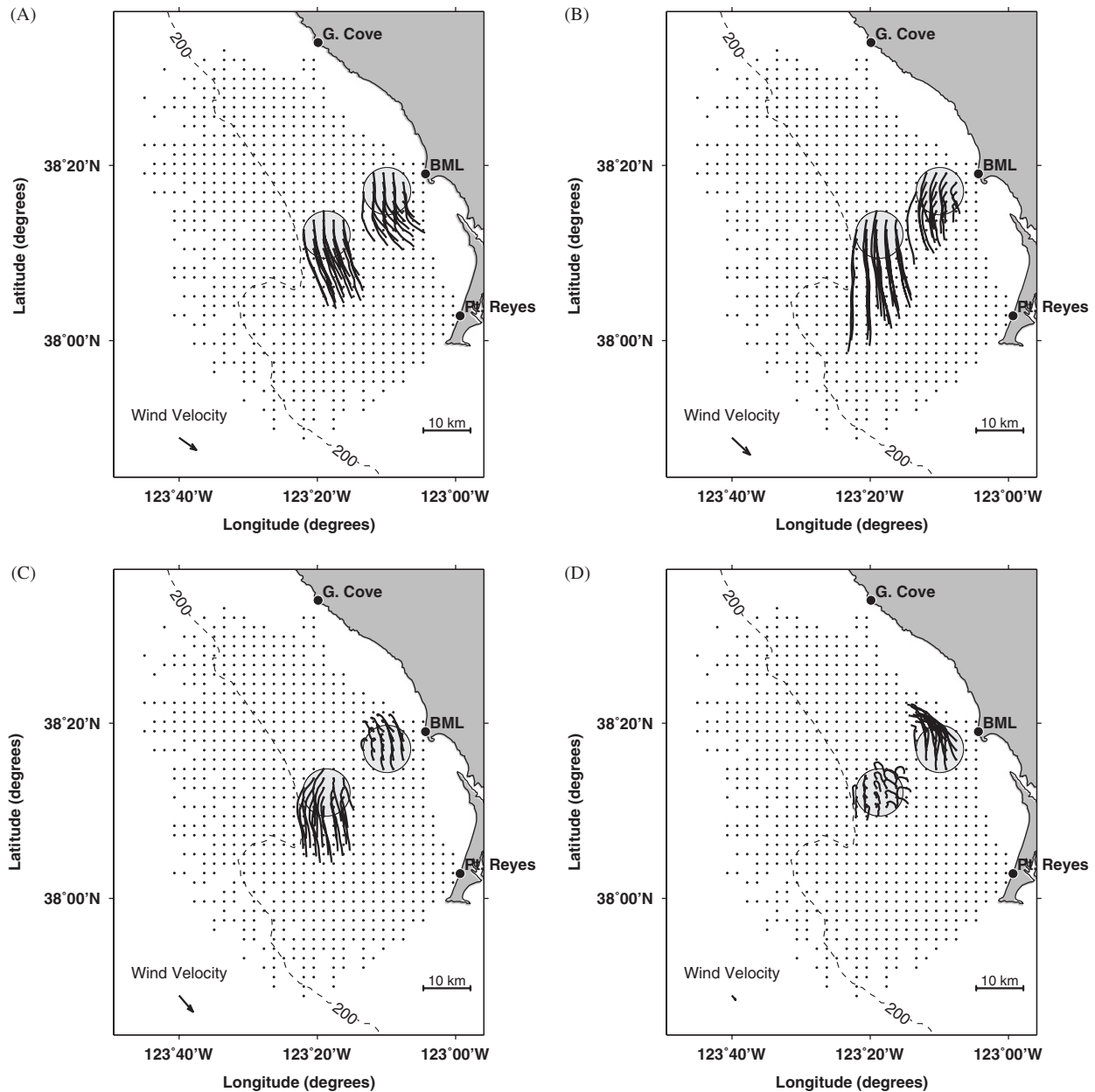


Fig. 8. Twelve-hour particle tracks from inner shelf and outer shelf zones during periods of upwelling and relaxation. Tracks begin at 00:00 GMT-8 on 7 (A), 16 (B), 18 (C), and 24 (D) of July 2003. Wind velocity at NDBC 46013 buoy is indicated in the lower-left corner of each panel.

approximately co-located with the D90 and D130 moorings, respectively; see Wilkerson et al., 2006), as well as from the southern zones.

The spatial distribution of possible displacements is plotted in Figs. 11A and D for parcels starting in the inner shelf or outer shelf zones, respectively. In both cases, a bimodal “dispersal” pattern is

obtained, with one mode representing equatorward transport and the other poleward or near-zero transport (Figs. 11A and D). The bimodal nature of the displacement pattern is persistent even if particles are followed for 2 days. Over the outer shelf, the vast majority of water parcels are transported southward, while, over the inner shelf,

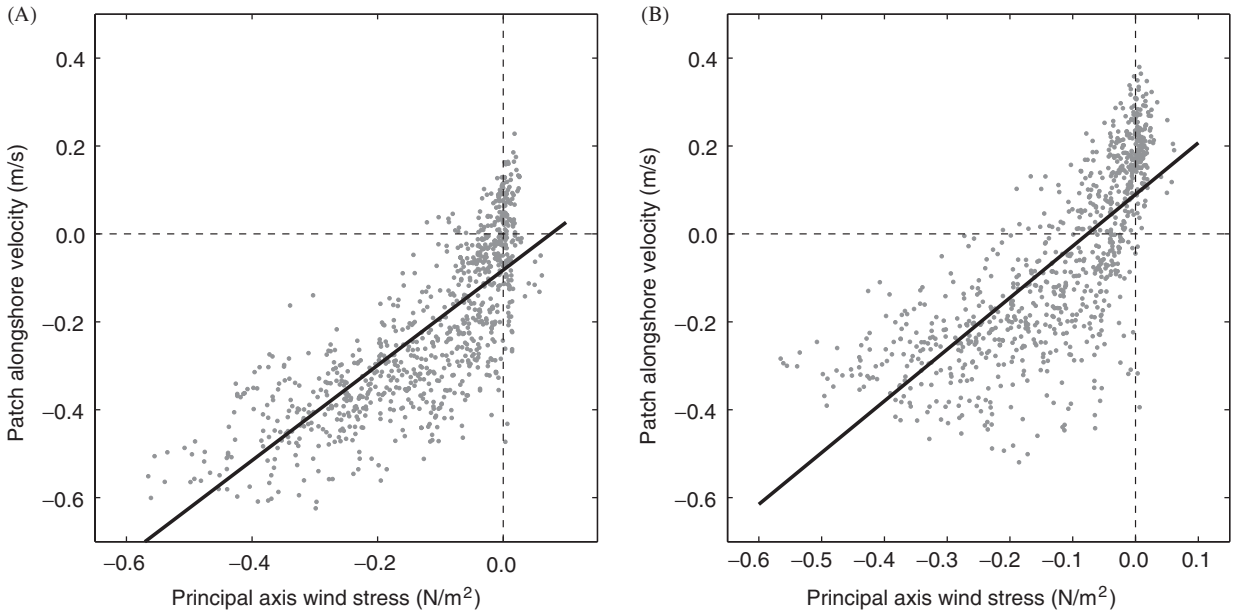


Fig. 9. Scatter plot of principal axis wind stress vs. alongshore velocity over a 12-h period (calculated simply as mean alongshore displacement/time) from the outer shelf (A) and inner shelf, (B) zones. Black, straight lines show lines of best fit calculated via linear regression. The regression in panel (A) explained 60% of the overall variance, while that in panel (B) explained 56%.

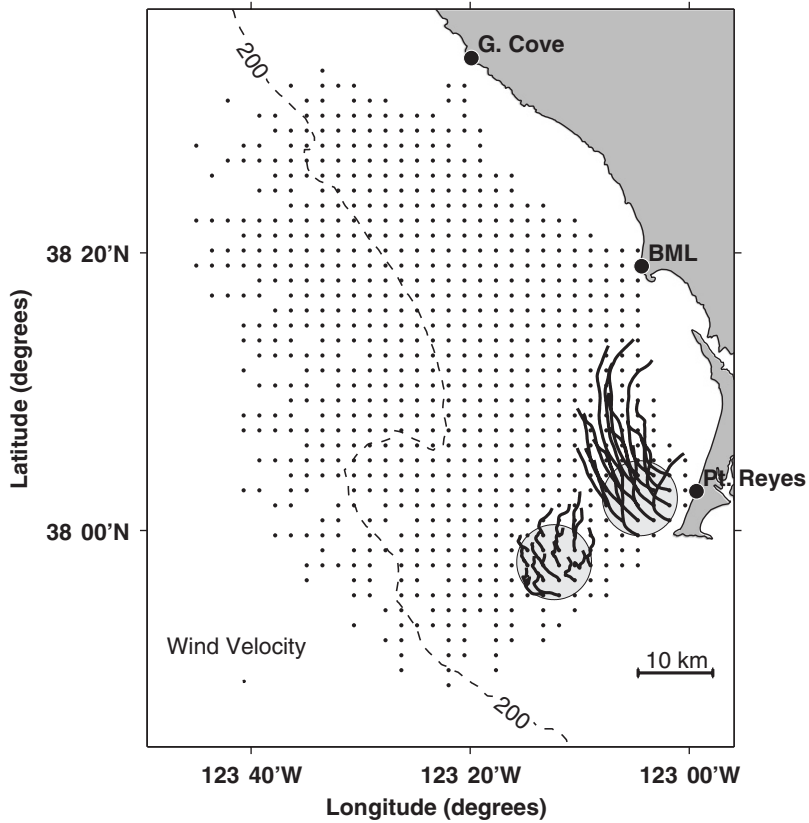


Fig. 10. Twelve-hour particle tracks from the Reyés offshore and Reyés inshore zones during a period of weak, relaxation-favorable winds (26 July 2003). Wind velocity at NDBC 46013 buoy is indicated in the lower-left corner of each panel.

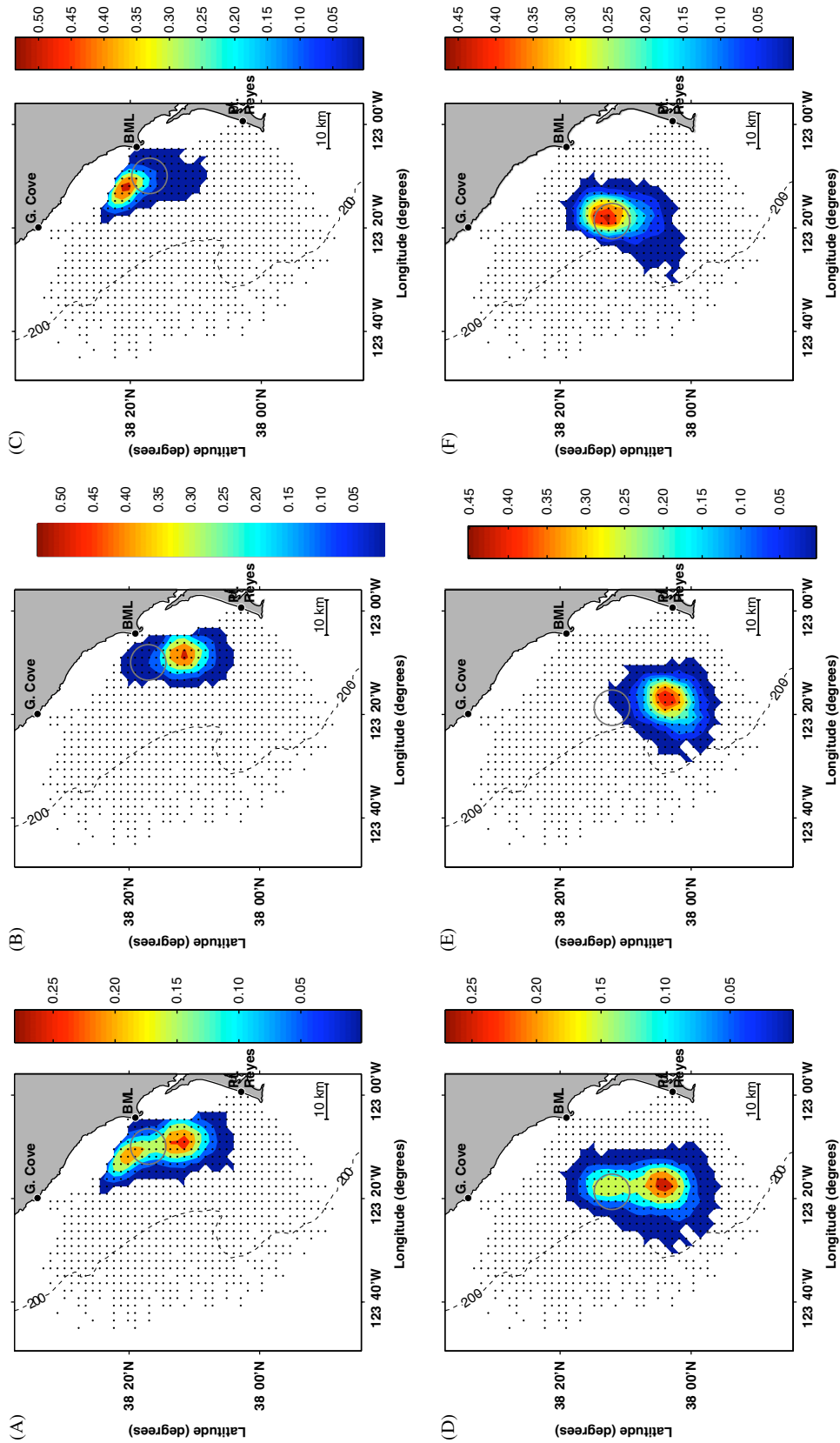


Fig. 11. Average particle movement patterns after 12 h at inner shelf (A–C) and outer shelf (D–F) zones. (A) and (D) show movements averaged over total time, (B) and (E) include just periods of considerable upwelling favorable winds (wind stress magnitude greater than  $0.15 \text{ N m}^{-2}$ ) and (C) and (F) include periods of weak winds (i.e. relaxation winds; stress less than  $0.05 \text{ N m}^{-2}$ ). Color indicates the percentage of time that at least one particle released in the zone was at a location after 12 h time, with red indicating the highest percentage. Color scales are different in each panel. Gray curves indicate the original position of water parcels.

the bimodal distribution is more marked and water parcels may be transported either poleward or equatorward.

The two modes of the distribution are shown to correspond to the reversal of flow between upwelling and relaxation conditions when the distribution of displacements is separated into “upwelling” and “relaxation” periods based on the wind stress. Identifying upwelling conditions by equatorward wind stress in excess of  $0.15 \text{ N m}^{-2}$ , the destination probability for parcels starting in upwelling conditions is plotted in Fig. 11B for origins in the inner shelf zone and in Fig. 11E for the outer shelf. The most probable outcome is that water in the inner shelf zone is found about 10 km south after 12 h, although displacement as much as 20 km south can be observed during upwelling. In comparison, water in the outer shelf zone is most likely to be found about 20 km south after 12 h, with maximum displacements of 30 km being observed. While there is only a small probability of being advected east or west of this dominant equatorward advection axis, there is more chance of westward (offshore) transport from the outer shelf zone than from the inner shelf zone. While there appear to be some upwelling scenarios in which transport from the outer shelf zone is near-zero and transport from the inner shelf zone is weakly northward, most of these realizations are for 12-h periods which start during relaxing upwelling winds, but before the wind stress has

dropped below  $0.15 \text{ N m}^{-2}$ . In the works of Largier et al. (1993) and Kaplan et al. (2005) it is shown that poleward relaxation flows can start during weakening upwelling winds that are still moderate in strength.

Under relaxation conditions (wind stress  $< 0.05 \text{ N m}^{-2}$ ), near-zero transport is observed over the outer shelf while the most probable outcome over the inner shelf is that water is found about 10 km up-coast after 12 h. While the range of possibilities is much the same over the inner and outer shelf (spread of destinations over 40 km under relaxation conditions), the mode is more dispersed for the outer shelf due to greater variability in currents under relaxation conditions. While currents over the inner shelf are reliably poleward during relaxation conditions, over the outer shelf currents can be either poleward or equatorward under relaxation conditions (Fig. 9; also see Kaplan et al., 2005, for more details). Some southward displacements are observed for transport started under relaxation conditions, but which change to upwelling conditions within a few hours. Over the outer shelf, these southward displacements may also occur during the 1st day of relaxed wind forcing, when equatorward currents continue over the outer shelf and slope.

Given the poleward, nearshore jet in the vicinity of Pt Reyes observed during relaxation conditions (Fig. 10), average trajectories are also explored for

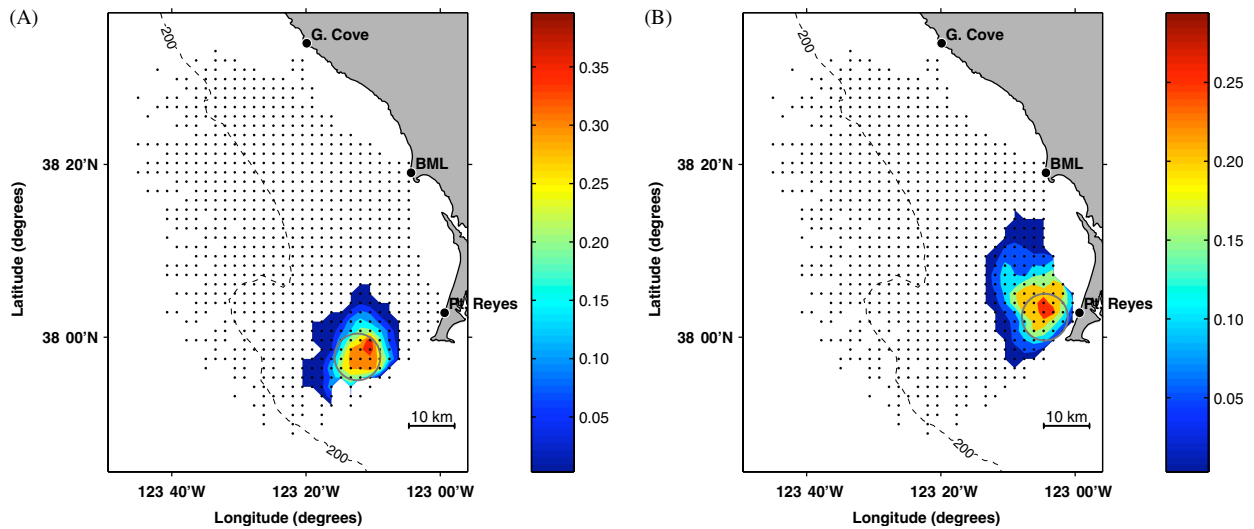


Fig. 12. Average particle movement during periods of weak, relaxation favorable winds after 12 h from Reyes offshore (A) and Reyes inshore (B) zones. Color indicates the percentage of time that at least one particle released in the zone was at a location after 12 h time. Gray curves indicate the original position of water parcels.

water parcels originating along the southern boundary of the HF radar domain (Fig. 12). While 12-h displacements of 5 km are most likely under relaxation conditions, at times water parcels from the Reyes inshore zone may be advected up to 20 km poleward in just 12 h (Fig. 12B). Not only is there strong poleward advection, but there appears to be very little offshore dispersion of these Reyes inshore waters during relaxation. In contrast, Reyes offshore waters are unlikely to be advected more than 10 km poleward (Fig. 12A). These waters are typically advected onshore and poleward with 5 km displacement towards the NE being most probable. Again, there is little probability of being dispersed offshore.

#### 4. Origin of surface waters observed in core WEST region

While the spatial extent of the HF radar domain limits the distance and time over which one can determine surface trajectories, one can look at the “origin” of water parcels by determining where these waters enter the radar domain. Ultimately, the interest is in the source of these waters in the sense of where they were brought to the surface and how they were transported to the core WEST region, as discussed in Section 7.2. Knowing where water has come from is critical to understanding its properties, including phytoplankton and zooplankton concentrations. Here we investigate the origin of water parcels by calculating “reverse trajectories” (Section 2.3)—tracks along which water parcels have been transported to the inner shelf and outer shelf zones of interest (i.e. key WEST study sites). We plot the probability of water from a given starting point on the domain boundary reaching the zone of interest within 4 days (Fig. 13). This does not mean that the zone is the ultimate destination (i.e. that the water parcel stops there), but that there is a link (connectivity) between the entry point and the zone of interest. In addition to the probability of connectivity (Fig. 13A and D), the typical travel time is shown in Fig. 13B and E, and the typical wind conditions under which the link is observed is shown in Fig. 13C and F.

The overwhelming majority of particles that reached the outer shelf zone entered the domain along the northern edge (Fig. 13D). On average, these particles took 1–2 days to travel from the edge to the zone of interest—about 15–25 km day<sup>-1</sup> (Fig. 13E). These northern origins occurred during

periods of upwelling favorable winds (Fig. 13F), with origins clustered off Gerstle Cove indicating reliable alongshore transport during strong wind forcing. Similar alongshore transport is seen in the origins for the inner shelf zone during strong upwelling winds (Fig. 13A and C), although the origins are more spread out due to the shape of the domain boundary. The proximity of the boundary is the primary control on travel time from the boundary, but displacements of order 10–15 km day<sup>-1</sup> are apparent. These results indicate upwelling sources of surface water along the coast north towards Pt Arena.

During relaxation, most inner-shelf surface waters originate in the south (accounting for about 40% of the total number of trajectories for all times) whereas origins are more varied for outer-shelf surface waters. The eastern and southeastern boundaries are likely origins for inner-shelf waters during relaxation (Fig. 13A and C). Consistent with the relaxation transport patterns described in Section 3, the travel times from Pt Reyes are of order 2 days (10–15 km day<sup>-1</sup>; Fig. 13B). In addition to these primary relaxation origins, it appears that inner-shelf surface waters may also originate from offshore during relaxation. Although uncommon, most origins are possible with long transit times of 3–4 days suggesting an indirect route—for example, based on the structure of the flow described in Section 3, one may expect waters with an origin due west of the destination zone would first move southward during upwelling and then be entrained into a northward relaxation flow. Similarly, waters originating along the southwestern edge of the domain under relaxation conditions are likely to move onshore (cf. Fig. 12A) and then be entrained into the nearshore poleward flow.

While surface waters in the outer-shelf zone may come from offshore or inshore during relaxation, there is no evidence of southern origins (Fig. 13D). The origins with strongest relaxation character are found along the offshore boundary, northwest of the destination zone (Fig. 13F). Although less common, this is a coherent origin with travel times of about 2 days, suggesting a direct route from origin to destination (about 10 km day<sup>-1</sup>). As noted in Section 3, equatorward flow may continue over the outer shelf and slope during relaxation periods; this result then suggests that an onshore component can also develop during relaxation. Closer examination of the individual trajectories that delivered particles from the northwestern edge of the domain

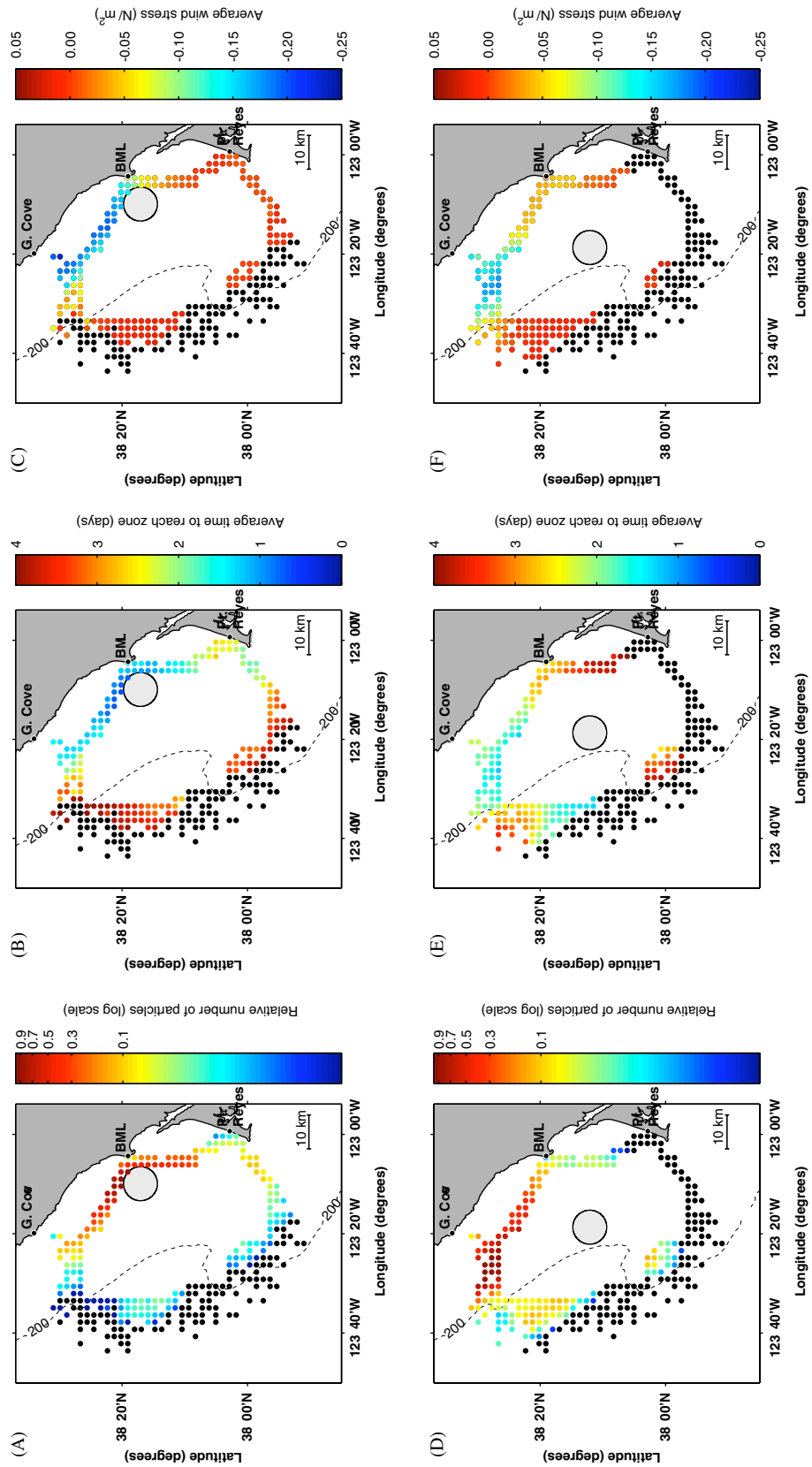


Fig. 13. Origins of particles reaching outer shelf (A–C) and inner shelf (D–F) zones. The zone for each panel is indicated by a gray circle. (A) and (D) show the number of particles from each border grid point reaching the respective zone in less than 4 days. Note that the color scales in (A) and (D) are logarithmic. (B) and (E) are the average time it took particles to reach the zone, and (C) and (F) are the average wind stress over the time period that particles were traveling from the edge of the data domain to the zone.

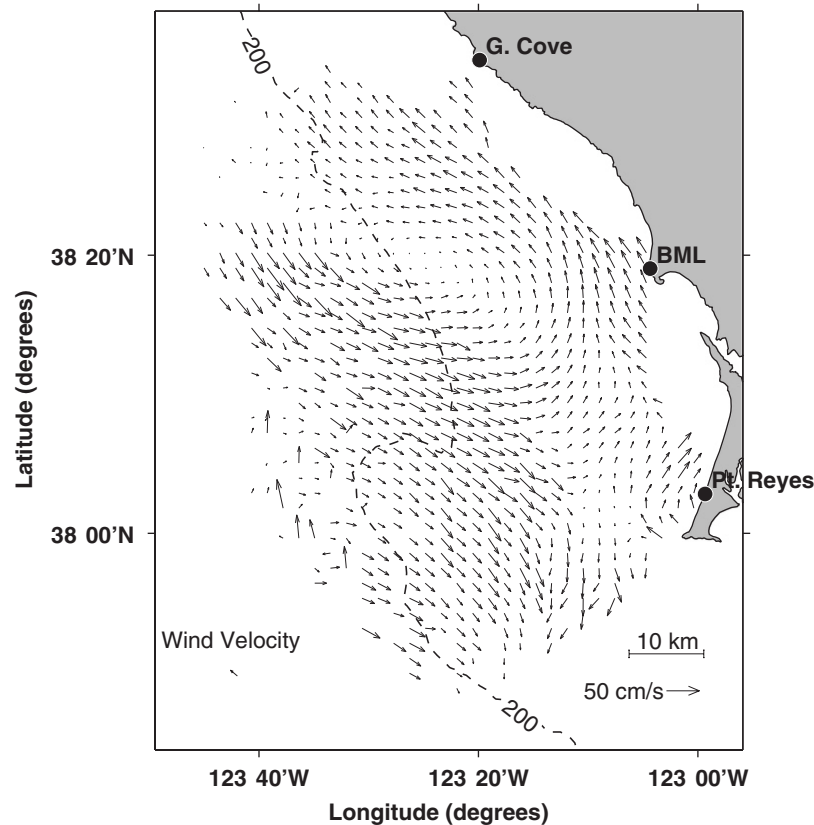


Fig. 14. Daily average surface currents from 20 August 2003. Winds at this time were weakly downwelling favorable (SE winds of  $3.3 \text{ m s}^{-1}$ , wind stress of  $0.015 \text{ N m}^{-2}$ ).

to the offshore zone confirmed this. The majority of these trajectories date from a single week-long period in late August (17–24), during which equatorward flow over the shelf edge meandered onshore west of Bodega Head and interacted with poleward flow over the inner-shelf (Fig. 14). Equatorward-flowing offshore waters were entrained onshore and into the poleward nearshore current, arriving a further 2 days later at the inner shelf destination zone.

##### 5. Destination of surface waters observed in core WEST region

As in the study of origin/source (Section 4), the spatial extent of the HF radar domain limits the distance and time over which one can determine surface trajectories. Thus, one can only look at the “destination” of surface water parcels in the sense of where these waters exit the radar domain. Ultimately, the interest is in the “fate” of these

waters, i.e. where they are eventually swept off the shelf or detrained in a coastal zone, as discussed in Section 7.4. Knowing where water goes is critical to understanding the fate of water-borne material, specifically phytoplankton and zooplankton concentrations observed at key WEST stations. Here we investigate the destination of water parcels as they are transported away from the inner shelf and outer shelf zones of interest (i.e. key WEST study sites). We plot the probability of waters exiting the radar domain within 6 days, and where they do so (Fig. 15), as well as the time to be exported (Fig. 16). Note that waters exported to inshore regions (numbers 4–6 on horizontal axis of Figs. 15 and 16) may be returned to the domain some time later (but this cannot be tracked), whereas waters exported along the southern edge of the data region by rapid equatorward currents are unlikely to be returned to the domain in the near future.

After 6 days, 85% of all water parcels that start in the inner or outer shelf zones are exported from the

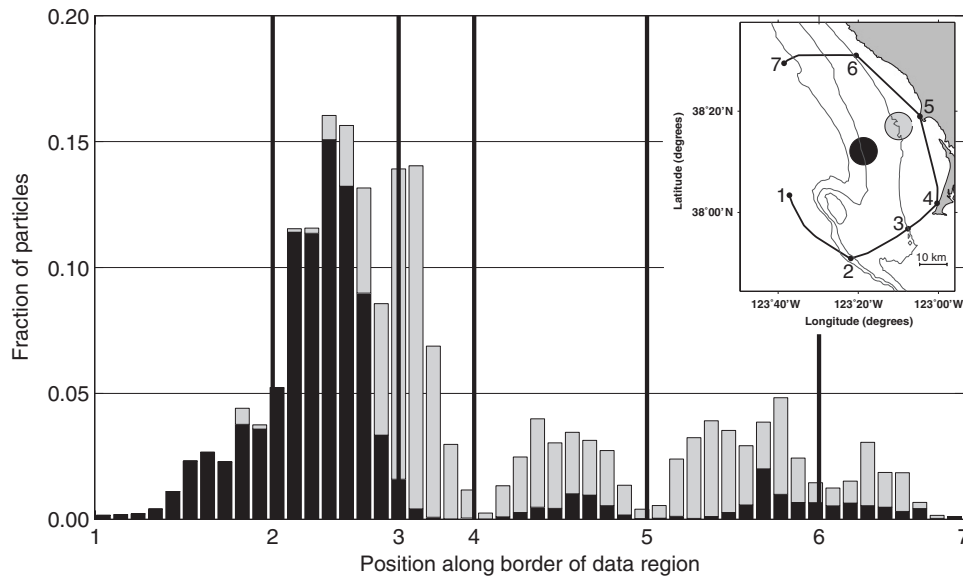


Fig. 15. Histogram of number of particles exiting the data region along different areas of the border. Black portion of bars are results for particles released from the outer shelf zone, while those for inner shelf zone are in gray. Horizontal axis is distance along the border of the data region, with numbers 1–7 corresponding to those seen in the inset in the upper, right-hand corner of the figure. In particular, numbers 4, 5 and 6 are close to the Point Reyes, BML and Gerstle Cove radar stations, respectively. Vertical axis shows fraction of particles from each zone that exited along each section of the border (i.e. the sum of the fractions in all bins is two, one for each zone).

radar domain. The overwhelming majority of parcels released from the outer shelf zone (about 70%) exit the domain through a narrow window along the southern boundary, south of Cordell Bank and more than 20 km from the tip of Point Reyes (Fig. 15). The destination of parcels from the inner shelf zone is not as singular due to the proximity of the domain boundary and the strength of poleward relaxation flows. Nevertheless, there is a clear mode representing preferential export of inner-shelf surface waters across the southern boundary within 20 km of Pt Reyes (Fig. 15)—this accounts for about 40% of waters originating in the inner shelf zone. The other inner-shelf waters were either exported to the north during relaxation periods (about 30%), entrained into the nearshore between Reyes and Bodega (about 20%) or, less often, exited along the southern border more than 20 km from Pt Reyes (about 10%).

Outer shelf waters were exported by equatorward flows after 1.5 days on average (Fig. 16A), representing a rapid and direct transport (about  $30 \text{ km day}^{-1}$ ). Export via other boundaries was far less likely and only after longer periods, suggesting weaker currents or current reversals. During upwelling conditions, inner shelf waters also were exported rapidly by equatorward flows, typically

within 2 days (Fig. 16B), representing displacements of order  $15\text{--}30 \text{ km day}^{-1}$ . During relaxation, inner shelf waters were exported by poleward flows, crossing either the inshore boundary north of Bodega or the northern boundary. Export times represent displacements of order 10–15 km in a day, indicating direct advection out of the domain. A significant proportion of inner shelf surface waters also exit the radar domain along the inshore boundary between Bodega and Reyes, with very variable time to destination. In time these waters will be returned to the radar domain and thus do not represent a true export from this shelf region, but rather inshore retention.

## 6. Surface divergence patterns

Surface currents can be used to calculate the surface divergence, which should be zero in the absence of vertical fluxes. Daily divergence maps are generally noisy due to the decrease in the signal-to-noise ratio when calculating the difference between current vectors. In order to isolate persistent, large-scale patterns of surface divergence, noise was removed from the subtidal current data by eliminating EOFs that explained only a small percent of

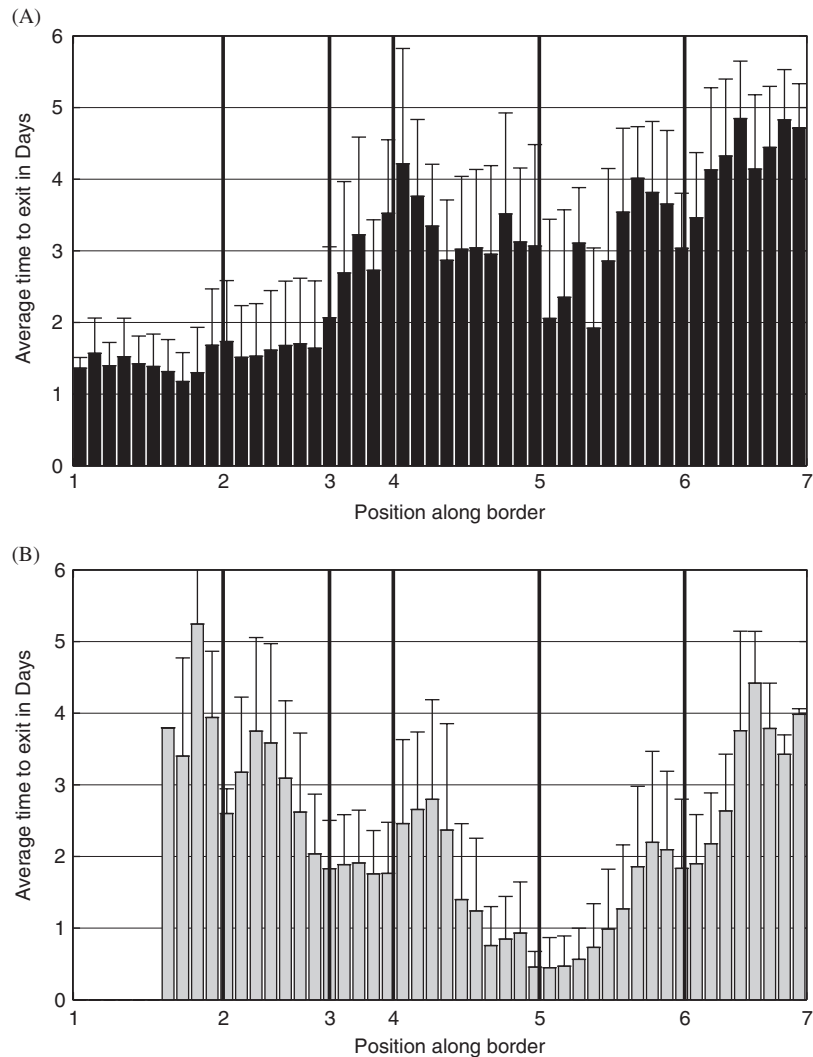


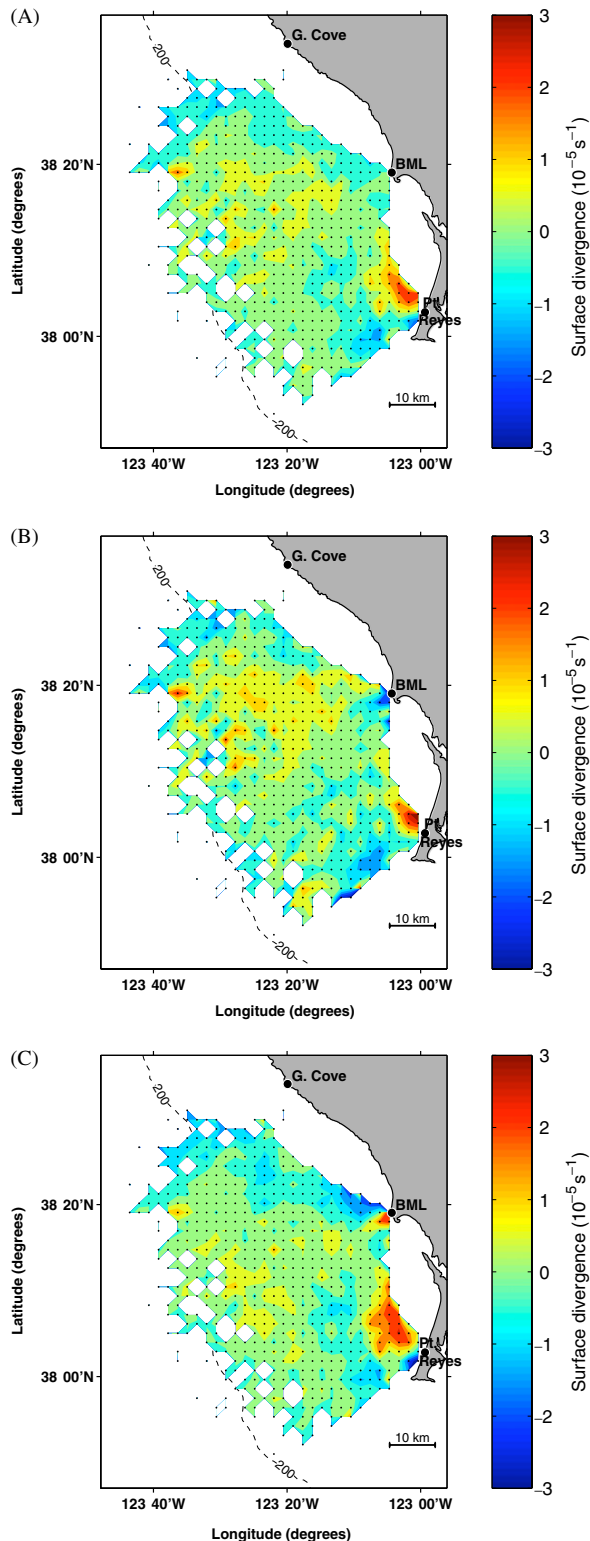
Fig. 16. Average time in days to travel from outer shelf (A) and inner shelf (B) zones to the edge of the data domain. Error bars are one standard deviation, and numbers along horizontal axis correspond to those in Fig. 14. In particular, numbers 4, 5 and 6 are close to the Point Reyes, BML and Gerstle Cove radar stations, respectively.

the overall variance before calculating the divergence.

The time-averaged surface divergence for subtidal and noise-reduced HF radar-derived currents averages out much of the possible structure. Values are low throughout the domain,  $< 2 \times 10^{-5} \text{ s}^{-1}$  everywhere other than in the zone of divergence immediately north of Pt Reyes (Fig. 17A). However, patterns emerge when the data are separated into upwelling and relaxation conditions. During upwelling conditions (Fig. 17B), there is an extensive region of positive divergence over the shelf off Bodega (i.e. in the northern half of the domain),

with maximum values over the outer shelf of order  $2 \times 10^{-5} \text{ s}^{-1}$ . This is consistent with the idea of wind-driven upwelling and observations from WEST moorings (Dever et al., 2006). However, with the exception of the localized divergence anomaly immediately north of Pt Reyes, the southeastern domain exhibits surface convergence (of order  $10^{-5} \text{ s}^{-1}$ ). This convergence indicates the absence of surface upwelling in this region and is likely due to the offshore flow curvature induced by Pt Reyes as a barrier to equatorward flow and the presence of onshore winds along the northern shore of the Pt Reyes peninsula (cf. a similar effect on

north side of Cape Mendocino, as described by Largier et al., 1993). This convergence is consistent with observations of warmer waters with higher



levels of chlorophyll along this coast, in contrast to coasts north of Bodega Head (Vander Woude et al., 2006).

The cause of the localized divergence during upwelling-favorable winds near Pt Reyes is unclear. It may be associated with residual poleward flow (relaxation flow) that can occur under nominal upwelling conditions (i.e. wind stress in excess of  $0.15 \text{ N m}^{-2}$ ), but there is likely also some error due to methodological difficulties associated with calculating the surface divergence near a radar. Close to the radars and along the line of sight between two radars, the accuracy of the component of the surface velocity perpendicular to the radial direction is low. This at times leads to exaggerated current velocities near the radars, perhaps explaining some or all of the surface divergence near Pt Reyes during upwelling conditions.

During relaxation conditions (Fig. 17C), there is a marked positive divergence region associated with the separation of poleward flow past Pt Reyes (e.g., Fig. 7B and Fig. 18), with a clockwise separation eddy often being observed. At the core, average values of up to  $2 \times 10^{-5} \text{ s}^{-1}$  are observed, while values in excess of  $1 \times 10^{-5} \text{ s}^{-1}$  extend 20 km north from Pt Reyes and 10 km offshore from Pt Reyes. As discussed above, methodological problems associated with calculating surface divergence near one of the radars could explain some of this positive divergence, but the spatial extent and consistency of this pattern indicate that it unlikely to be entirely the result of error. This divergence zone represents either a thinning of the surface layer or a significant vertical flux into the surface flow. Offshore of Pt Reyes, a zone of weak convergence is observed (Fig. 17C), associated with curvature in the poleward flow as it encounters the equatorward flowing offshore waters. Coherent convergence is also seen along a swath extending northwest from Bodega, associated with curvature in the poleward flow as it encounters the more northwest oriented coast north of Bodega, though it is difficult to assess the robustness of this feature given the proximity to the domain boundary and the line of sight between the BML and Gerstle Cove radars.

Fig. 17. Average surface divergence for (A) all periods, (B) periods of upwelling-favorable winds and (C) periods of weak, relaxation-favorable winds. Divergence was calculated using subtidal current data that had been reduced to the mean plus those empirical orthogonal functions that represented more than 5% of the overall variance (in this case the first four EOFs).

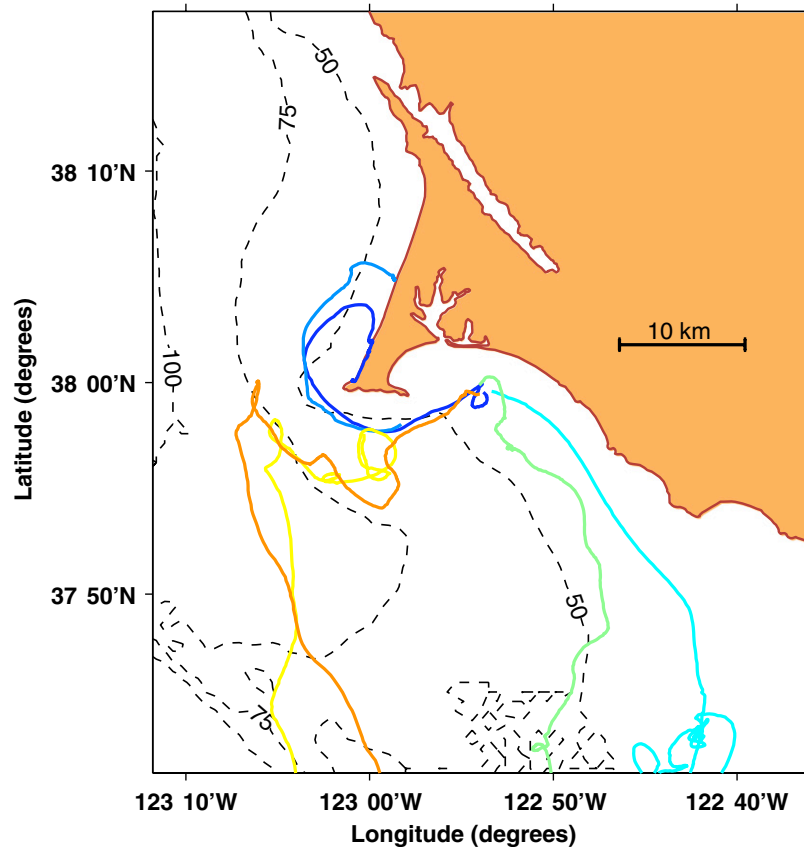


Fig. 18. WEST drifters from 2001 released south of Point Reyes. Drifter tracks are shown in colored lines and date from 19 May to 11 June 2001. Two drifters (shown in dark and medium blue) released on 19 May 2001 from Drake's Bay (south of Point Reyes) during a period of relaxation in wind strength impacted on the northern side of Point Reyes in less than a week.

Surface divergence for the region between Bodega and Reyes, inshore of the radar domain (southern light-gray area in Fig. 6), can be determined by calculating the line integral of currents normal to the boundary, i.e. the net inflow or outflow of surface waters. Dividing this net surface outflow by the surface area of the “Bodega embayment” provides an estimate of surface divergence averaged over this region (Section 2.4). The mean value over the entire spring–summer period was small (Table 1), consistent with the mean surface divergence map shown in Fig. 17A, and the mean value was much smaller than the standard deviation. During upwelling conditions, surface divergence in the embayment remained small and positive ( $0.16 \times 10^{-5} \text{ s}^{-1}$ ), indicating weak upwelling in the bay, while a distinct surface convergence was observed during relaxation conditions ( $-0.50 \times 10^{-5} \text{ s}^{-1}$ ). A similar calculation was made for the Russian River embayment (northern light-gray area in Fig. 6), and, while results indicated

Table 1

Mean and standard deviation of surface velocity divergence or flux per unit area for two embayments inshore of the HF-Radar domain

Embayment	Surface divergence for embayments					
	All times		Upwelling		Relaxation	
	Mean	Std. dev.	Mean	Std. dev.	Mean	Std. dev.
Bodega	-0.12	0.66	0.17	0.50	-0.57	0.65
Russian River	-0.07	0.63	0.18	0.50	-0.39	0.67

Values are given for all times, for upwelling periods and for relaxation periods. All values have units of  $10^{-5} \text{ s}^{-1}$ .

the same trend towards divergence during upwelling conditions and convergence during downwelling conditions (Table 1), the absence of nearshore radar data off Gerstle Cove potentially introduced large error in estimates of surface divergence for this

inshore region and these results are not discussed further.

The large variability in net surface divergence for the Bodega embayment was explored by separating the net influx and the net outflux, and then looking at the time dependence of these components and of the net divergence in relation to the time-varying wind forcing. The surface outflux is well correlated with wind forcing (correlation of  $-0.66$ ), but there is no correlation between influx and wind forcing. The largest surface divergence values were negative (i.e. convergence) and of order  $-2 \times 10^{-5} \text{ s}^{-1}$ . During 565 upwelling, divergence values were mostly positive, but weak, with most values less than  $0.5 \times 10^{-5} \text{ s}^{-1}$ . The wind-divergence correlation was marginally significant at  $-0.39$ .

## 7. Discussion

### 7.1. Plankton transport patterns

HF radar-derived trajectories for surface water parcels show a bimodal pattern with equatorward transport during upwelling winds and poleward transport during wind relaxations, consistent with the results of earlier mooring-based studies (e.g., Winant et al., 1987; Largier et al., 1993). However, transport of specific water properties or water-borne material, such as phytoplankton, may not exhibit the same spatial probability patterns as that for the transport of water mass. The aggregated transport of water-borne material depends also on the time-dependent concentration at the starting point, which is controlled not only by advection to that location but also by non-conservative processes such as primary production. The net transport is a cross product of time-dependent concentration and time-dependent displacement/transport. For example, preliminary results in Wilkerson et al. (2006) and Largier et al. (2006) indicate that higher chlorophyll fluorescence and diatom abundance are observed under relaxation conditions (see also Fig. 1), suggesting that the trajectories of upwelled waters, bloom time scales, and stratification could be important factors in determining locally observed phytoplankton densities (cf. Wieters et al., 2003). If this proves to be true in subsequent work, then there is a net poleward transport of chlorophyll and diatoms over the inner/mid-shelf off Bodega Bay, in spite of near-zero or weak equatorward net mass flux. This is consistent with the net poleward heat flux observed by Dever and Lentz (1994)

during SMILE—due to the tendency for warmer water (greater heat concentration) during periods of poleward flow. In contrast to the inner/mid-shelf, during relaxation conditions over the outer shelf there is near-zero advection whereas equatorward advection is strong during upwelling conditions, such that one expects a net equatorward transport of diatoms/chlorophyll irrespective of the time-dependence of diatom/chlorophyll concentration. These ideas will be explored quantitatively in future work.

### 7.2. Surface divergence and vertical fluxes

As noted previously (Section 2), the radar-derived surface flow patterns provide a measure of surface velocity divergence, which may be different to surface transport divergence if there are strong gradients in the depth of the surface layer. However, sudden changes in surface mixed-layer depth are not expected in the absence of fronts, which are usually associated with the meeting of two distinct water masses or with the interaction of flow with abrupt topography. With the possible exception of the Pt Reyes separation eddy observed during poleward flow, it is reasonable to assume the absence of sudden changes in surface-layer depth in the WEST region and to interpret surface velocity patterns as surface transport patterns. In WEST, the mooring-derived transport divergence estimates of  $4\text{--}20 \times 10^{-5} \text{ m s}^{-1}$  (Dever et al., 2006) compare well with the radar-derived velocity divergence estimates of  $0\text{--}2 \times 10^{-5} \text{ s}^{-1}$  (Fig. 17), given a surface mixed layer of order 10 m, as observed. Furthermore, the alongshore position of the cross-shore boundary between positive divergence to the north of Bodega Head and convergence to the south during upwelling periods (Fig. 17B) agrees roughly with the southern end of the wind maximum due to the Pt Arena wind expansion fan (Winant et al., 1987; Koracin and Dorman, 2001) and with the tendency for warmer waters and higher chlorophyll levels to be observed south of this latitude and approaching the north shore of Pt Reyes (Vander Woude et al., 2006).

A rough estimate of the relative strengths of vertical and horizontal volume fluxes can be obtained from comparing the surface velocity divergence with the surface velocity: the proportion of vertically entrained water is given by (velocity difference)/velocity. Thus, during upwelling conditions, the equatorward flow past Bodega of about

$0.2\text{--}0.4\text{ m s}^{-1}$  experiences divergence of order  $1 \times 10^{-5}\text{ s}^{-1}$  over a distance of some 20 km, resulting in a vertical volume flux comparable in magnitude to the horizontal flux. In other words, under these conditions, of the waters sampled at biological survey station D3 (center of outer shelf zone), roughly half of the water entered the radar domain along the northern boundary and half was entrained from sub-surface as surface waters moved south through this divergence region. Similarly, if the surface velocity divergence immediately north of Pt Reyes is not due to changes in surface layer depth (or methodological problems, as discussed in Section 6), then the associated transport divergence would entrain a volume flux of sub-surface water comparable with the volume flux of waters being advected poleward past Pt Reyes. Thus, the water sampled at station D2 (co-located with D90 mooring, which is at the center of the inner shelf zone) would be composed of significant quantities of both surface waters from the Farallons and waters entrained from depths 635 below the surface layer (i.e. upwelled waters).

Conversely, areas of convergence represent locations where the surface mixed layer is thickening, surface waters are being subducted or surface waters are being entrained out of the surface layer. The primary areas of convergence appear to be where flow converges on the land (e.g., north of the Reyes peninsula during equatorward flow; north of Bodega during poleward flow) or converges with a counter current (e.g., where poleward flow around Pt Reyes meets the equatorward flow over the outer shelf during relaxation periods).

The estimates of net divergence in the Bodega embayment also provide an idea of the strength of upwelling (vertical flux into surface waters). Surface divergence during upwelling conditions of order  $0.2 \times 10^{-5}\text{ s}^{-1}$  is markedly weaker than over the shelf off Bodega and comparable with the near-zero values over the mid-shelf between Bodega and Reyes—indicating suppressed upwelling in this region. In addition to divergence, the outflux and influx data provide an estimate of the rate of exchange of surface waters between this nearshore region and the open shelf. These estimates are of the order of a day, indicating that the embayment as a whole may not offer any specific retention opportunities. However, this does not preclude retention in parts of the bay or through sub-surface circulation features (e.g., Roughan et al., 2005). The strong correlation of surface outflux from the embayment

with wind is in contrast to that for influx and wind, suggesting somewhat different mechanisms for the two processes. While upwelling wind events typically result in a burst of surface outflow, periods of strong inflow may occur during either upwelling wind events (inflow from the north) or relaxation events (inflow from the south), explaining the lack of correlation between surface influx and wind.

Furthermore, a number of the most important influx events were observed early during relaxation periods when a strong influx is not matched by an outflux and downwelling can be expected.

### 7.3. Sources of surface water off Bodega Bay

Following the recognition of a bimodal flow pattern off Bodega, with upwelling and relaxation modes, the surface waters sampled at WEST stations off Bodega appear to have two primary origins—entering the radar domain in the north during upwelling conditions and entering the radar domain nearshore in the south during relaxation conditions (Section 4). The identification of two primary origins indicates, in turn, that there are likely two primary sources of surface waters.

During upwelling conditions waters have a northerly source, with the orientation of flow towards the outer shelf zone, suggesting that waters may originate in the core of the upwelling cell of Pt Arena. While there is no evidence of any offshore source contributing to the shelf off Bodega under upwelling conditions, radar-based estimates of surface divergence suggest that considerable volumes of sub-surface water are entrained into the equatorward flowing waters (e.g., from Section 7.2, roughly equivalent horizontal and vertical fluxes for surface waters passing through the upwelling zone over the shelf north of Bodega en-route to the outer shelf zone). The origin of surface waters sampled in the inner shelf zone (Fig. 13A) indicates that these waters are likely upwelled along the coast immediately north of Bodega (i.e. south of Gerstle Cove). Preliminary hydrographic analyses (Largier et al., 2006) find that these northerly waters are “upwelled waters” in that their characteristics are low temperature and high salinity (cf. Schwing et al., 1997).

During relaxation, warmer waters, which are also often of lower salinity, are observed off Bodega (Largier et al., 2006), suggesting either an offshore or a Gulf of Farallons source (cf. Schwing et al., 1997; Wing et al., 1998). The dominance of southerly origins for the inner shelf zone during

relaxation conditions suggests that these surface waters have a source in the Farallons (Fig. 13A and C). Although the radar data does not extend beyond Pt Reyes, two drifters released in the northern Gulf of the Farallons at the start of a relaxation event in May 2001 provide a clear demonstration of nearshore Farallons waters being transported around Pt Reyes in a strong jet (Fig. 18). The strong surface divergence in the separation feature immediately north of Pt Reyes (Fig. 17C) suggests that significant volumes of sub-surface water are also entrained into these poleward-flowing waters. Water parcel origins from further offshore suggest that waters from the outer Gulf of Farallons, offshore oceanic waters and upwelled waters also may be entrained into the poleward flow that delivers surface waters to the inner shelf zone, 700 though in relatively limited quantities. The long transit time from the origin along the offshore west boundary of the radar domain suggests that these waters are likely to be equatorward-moving upwelled waters that are subsequently entrained into the poleward-moving relaxation flow over the inner/mid-shelf.

The source of surface waters at the outer shelf zone during relaxation is not in the south (Fig. 13D) and the transport pattern is less clear. Nearshore and offshore origins are both possible. Investigation of the offshore origins of surface waters at the outer shelf zone during relaxation revealed that these origins came from a single limited time period, suggesting that this might be an unusual event. It remains to be determined how recurrent these events are over multiple years.

#### 7.4. Fate of surface water off Bodega Bay

The ultimate fate of surface waters sampled at WEST stations off Bodega may be deduced from the radar-derived destinations along the boundary of the radar domain. The fate of surface waters during strong upwelling is to be exported from the Bodega shelf region via a rapid equatorward current that detaches from the shoreline at Pt Reyes. It is unlikely that these waters return to the domain, unless they are detrained from the upwelling jet and enter the northern Gulf of Farallons. Thus, it is expected that waters starting over the outer shelf will be effectively exported from the shelf (in the absence of a relaxation event en-route), while waters that start over the inner shelf may travel close to Pt Reyes and be detrained into the northern Farallons.

Both scenarios were observed during upwelling conditions for selected drifters deployed over the outer and inner shelf off Bodega, respectively.

The fate of surface waters during relaxation events is less clear from this analysis of radar data. While average transport patterns in the domain are clear, with poleward flow over the inner/mid-shelf and near-zero advection over the outer shelf (Figs. 13 and 15), it is not clear what happens beyond the radar domain. Relaxation events are usually short-lived and seldom can one invoke a quasi-steady flow pattern. With the return of upwelling winds following relaxation, it is expected that the surface waters over the shelf will be advected offshore rapidly due to near-surface stratification and enhanced Ekman velocities (cf. Lentz and Largier, 2006). This scenario was observed by selected drifter tracks over the shelf off Bodega. In this case, the fate of shelf surface waters will be offshore advection and vertical mixing into the incipient upwelling.

Although the fate of the majority of surface waters lies beyond the radar domain, a significant proportion of these waters may be retained within the domain, particularly when upwelling and relaxation phases are short-lived. Of the water parcels tracked to obtain the destination results plotted in Fig. 15, as much as 15% of the water remained within the domain after 6 days, mostly from periods when there are alternating upwelling and relaxation conditions. Depending on the distribution of this retained water, and the proportion of waters exported into the nearshore (i.e. retained in the nearshore), on the order of 2% of these surface waters may remain on the shelf in the Bodega area after 12 days—a period comparable with the planktonic larval duration of many benthic invertebrates (Grantham et al., 2003). This retention could have important consequences for larval settlement and population dynamics in the area.

## 8. Summary

Analysis of HF radar data on surface transport off Bodega points to a bimodal system, with equatorward transport throughout the shelf during upwelling winds and poleward transport over the inner/mid-shelf during relaxation. This pattern of transport shows up in both the origin and destination of waters sampled at key WEST moorings. During upwelling, waters stream south from the vicinity of the Pt Arena upwelling center, moving to the outer shelf zone near the D130

mooring (a.k.a. D3 biological survey station) and then on to the south of the radar domain, where they are exported from the domain and likely exported from the shelf via the Pt Reyes upwelling jet. Meanwhile, there is a substantial but weaker equatorward flow over the inner/mid-shelf, which reverses rapidly as wind stress weakens, even before a zero wind is achieved (Fig. 9B). This poleward flow over the mid/inner-shelf entrains not only waters from the Gulf of Farallones, but also some offshore waters, some upwelled waters from the north, some nearshore waters and some water from depth. Surface velocity divergence estimates compare reasonably with mooring-based estimates and indicate upwelling vertical fluxes in this region. The surface divergence pattern indicates enhanced upwelling along the open coast north of Bodega, and suppressed upwelling immediately north of the Reyes-Tomales headland, consistent with the tendency for warmer waters with higher chlorophyll concentrations in this locale (Vander Woude et al., 2006).

In subsequent work, we will combine radar-derived pathways developed in this paper with detailed data on nutrient and phytoplankton concentrations. By integrating these two elements, we hope to better understand the dynamics of algal blooms and to quantify the relative importance of transport and in situ production processes in accounting for coastal primary productivity in the area.

### Acknowledgments

The study has been supported by NSF CoOP Project Grant OCE-9907884. The authors would like to thank Bruce Nyden and Deedee Shideler for maintenance of the radar equipment and making the current data accessible, Clive Dorman for assistance with the wind data, and Mike Cook for the use of his HFRadarmap Matlab Toolbox. Louis W. Botsford, Cathy Lawrence, Ed Dever and the rest of our WEST colleagues gave many useful suggestions in the preparation of this manuscript. Jeff Paduan has been extremely forthcoming with advice and suggestions. This manuscript is contribution #2272 of the Bodega Marine Laboratory, University of California at Davis.

### References

Beardsley, R., Limeburner, R., Rosenfeld, L., 1985. CODE-2: moored array and large-scale data report. In: Woods Hole

- Oceanographic Institute Technical Report WHOI-85-35, Woods Hole Oceanographic Institute, MA, pp. 1–21.
- Bennett, J.R., Clites, H., 1987. Accuracy of trajectory calculation in a finite difference circulation model. *Journal of Computational Physics* 68 (2), 272–282.
- Chapman, R.D., Graber, H.C., 1997. Validation of HF radar measurements. *Oceanography* 10 (2), 76–79.
- Dever, E.P., Lentz, S.J., 1994. Heat and salt balances over the northern California shelf in winter and spring. *Journal of Geophysical Research-Oceans* 99, 16001–16017.
- Dever, E.P., Dorman, C.E., Largier, J.L., 2006. Surface boundary layer variability during spring and summer upwelling. *Deep-Sea Research II*, this issue [doi:10.1016/j.dsr2.2006.09.001].
- Dorman, C.E., Dever, E.P., Largier, J.L., Koracin, D., 2006. Buoy measured wind, wind stress and curl of the wind stress over the shelf off Bodega Bay, California. *Deep-Sea Research II*, this issue [doi:10.1016/j.dsr2.2006.07.006].
- Grantham, B.A., Eckert, G.L., Shanks, A.L., 2003. Dispersal potential of marine invertebrates in diverse habitats. *Ecological Applications* 13, S108–S116.
- Kaplan, D.M., Largier, J.L., Botsford, L.W., 2005. HF radar observations of surface circulation off Bodega Bay (Northern California, USA). *Journal of Geophysical Research* 110, C10020 [doi:10.1029/2005JC002959].
- Koracin, D., Dorman, C.E., 2001. Marine atmospheric boundary layer divergence and clouds along California in June 1996. *Monthly Weather Review* 129, 2040–2056.
- Large, W.G., Pond, S., 1981. Open ocean momentum flux measurements in moderate to strong winds. *Journal of Physical Oceanography* 11 (3), 324–336.
- Largier, J.L., Magnell, B.A., Winant, C., 1993. Subtidal circulation over the Northern California shelf. *Journal of Geophysical Research* 98 (C10), 18147–18179.
- Largier, J.L., Lawrence, C.A., Roughan, M., Kaplan, D.M., Dever, E.P., Dorman, C.E., Kudela, R.M., Bollens, S.M., Wilkerson, F.P., Dugdale, R.C., Botsford, L.W., Garfield, N., Kuebel Cervantes, B., Koracin, D., 2006. WEST: a Northern California study of the role of wind-driven transport in the productivity of coastal plankton communities. *Deep-Sea Research II*, this issue [doi:10.1016/j.dsr2.2006.08.018].
- Lentz, S.J., Largier, J.L., 2006. The influence of wind forcing on the Chesapeake Bay buoyant coastal current. *Journal of Physical Oceanography* 36 (7), 1305–1316.
- Lipa, B., 2003. Uncertainties in SeaSonde Current Velocities. In: Proceedings of the IEE/OES Seventh Working Conference on Current Measurement Technology. IEEE, San Diego, CA, pp. 95–100.
- Roughan, M., Mace, A.J., Largier, J.L., Morgan, S.G., Fisher, J.L., 2005. Subsurface recirculation & larval retention in the lee of a small headland: a variation on the upwelling shadow theme. *Journal of Geophysical Research* 110 (C10), C10027.
- Schwing, F.B., Hayward, T.L., Sakuma, K.M., Murphree, T., Mascarenas, A.S., Castillo, S.I.L., Mantyla, A.W., Cummings, S.L., Chavez, F.P., Baltz, K., Ainley, D.G., 1997. The state of the California current, 1996–1997: mixed signals from the tropics. *CalCOFI Reports* 38, 22–47.
- Vander Woude, A.J., Largier, J.L., Kudela, R.M., 2006. Nearshore retention of upwelled waters north and south of Point Reyes (Northern California)—Patterns of surface temperature and chlorophyll observed in CoOP WEST.

- Deep-Sea Research II, this issue [[doi:10.1016/j.dsr2.2006.07.003](https://doi.org/10.1016/j.dsr2.2006.07.003)].
- Wieters, E., Kaplan, D.M., Navarrete, S.A., Sotomayor, A., Largier, J.L., Nielsen, K., Veliz, F., 2003. Alongshore and temporal variability in chlorophyll-*a* concentration in Chilean nearshore waters. *Marine Ecology Progress Series* 249, 93–105.
- Wells, D., Beck, N., 1987. Guide to GPS positioning, second print. Canadian GPS Associates, Fredericton, NB, Canada.
- Wilkerson, F.P., Dugdale, R.C., Marchi, A., Hogue, V., Lassiter, A., 2006. The phytoplankton bloom response to wind events and upwelled nutrients during the CoOP-WEST Study. *Deep-Sea Research II*, this issue [[doi:10.1016/j.dsr2.2006.07.007](https://doi.org/10.1016/j.dsr2.2006.07.007)].
- Winant, C.D., Beardsley, R.C., Davis, R.E., 1987. Moored wind, temperature, and current observations made during Coastal Ocean Dynamics Experiments 1 and 2 over the Northern California continental shelf and upper slope. *Journal of Geophysical Research* 92, 1569–1604.
- Wing, S.R., Botsford, L.W., Ralston, S.V., Largier, J.L., 1998. Meroplanktonic distribution and circulation in a coastal retention zone of the northern California upwelling system. *Limnology and Oceanography* 43, 1710–1721.